Applied Geography 63 (2015) 1–8

Contents lists available at ScienceDirect

Applied Geography

journal homepage: www.elsevier.com/locate/apgeog

Spatiotemporal patterns of tropical deforestation and forest degradation in response to the operation of the Tucuruí hydroelectric dam in the Amazon basin

Gang Chen [a, *], Ryan P. Powers [b], Luis M.T. de Carvalho [c], Brice Mora [d]

[a] Department of Geography and Earth Sciences, University of North Carolina at Charlotte, 9201 University City Blvd, Charlotte, NC 28223, USA
[b] Department of Ecology and Evolutionary Biology, Yale University, 165 Prospect Street, New Haven, CT 06520, USA
[c] Department of Forest Sciences, Federal University of Lavras, 37200-000 Lavras, Brazil
[d] Global Observation for Forest Cover and Land Dynamics (GOFC/GOLD) Land Cover Project Office, Wageningen University and Research Centre, 6700 AA Wageningen, The Netherlands

ARTICLE INFO

Article history:
Received 17 April 2015
Received in revised form
3 June 2015
Accepted 3 June 2015
Available online

Keywords:
Deforestation
Forest degradation
Hydroelectric dam
Spatiotemporal pattern
Amazon basin
Remote sensing
GIS
Statistical analysis

ABSTRACT

The planned construction of hundreds of hydroelectric dams in the Amazon basin has the potential to provide invaluable 'clean' energy resources for aiding in securing future regional energy needs and continued economic growth. These mega-structures, however, directly and indirectly interfere with natural ecosystem dynamics, and can cause noticeable tree loss. To improve our understanding of how hydroelectric dams affect the surrounding spatiotemporal patterns of forest disturbances, this case study integrated remote sensing spectral mixture analysis, GIS proximity analysis and statistical hypothesis testing to extract and evaluate spatially-explicit patterns of deforestation (clearing of entire forest patch) and forest degradation (reduced tree density) in the 80,000 km^2 neighborhoods of the Brazil's Tucuruí Dam, the first large-scale hydroelectric project in the Amazon region, over a period of 25 years from 1988 to 2013. Results show that the average rates of deforestation were consistent during the first three time periods 1988–1995 (620 km^2 per year), 1995–2001 (591 km^2 per year), and 2001–2008 (660 km^2 per year). However, such rate dramatically fell to half of historical levels after 2008, possibly reflecting the 2008 global economic crisis and enforcement of the Brazilian Law of Environmental Crimes. The rate of forest degradation was relatively stable from 1988 to 2013 and, on average, was 17.8% of the rate of deforestation. Deforestation and forest degradation were found to follow similar spatial patterns across the dam neighborhoods, upstream reaches or downstream reaches at the distances of 5 km–80 km, suggesting that small and large-scale forest disturbances may have been influencing each other in the vicinity of the dam. We further found that the neighborhoods of the Tucuruí Dam and the upstream region experienced similar degrees of canopy loss. Such loss was mainly attributed to the fast expansion of the Tucuruí town, and the intensive logging activities alongside major roads in the upstream reservoir region. In contrast, a significantly lower level of forest disturbance was discovered in the downstream region.

1. Introduction

Tropical forests absorb carbon at a level greater than all the other types of forests combined, storing a total amount of 471 ± 93 Pg (Pan et al., 2011). However, deforestation and forest degradation are prevalent in the tropical regions as well, accounting for 32% of the global tree loss, at the rate of 2010 km^2 per year (Hansen et al., 2013; Saatchi et al., 2011). While natural disturbances can affect forest ecosystem structure and function, anthropogenic activities, mostly in the form of land use conversion, are widely considered the dominant drivers of contemporary forest cover change (Fuller, Foster, McLachlan, & Drake, 1998; Lambin, 1997; Uriarte et al., 2009). Recognition of the uniqueness of tropical forests, with respect to both its ecological value and high conservation importance, has inspired debate around their protection and what level of anthropogenic activity is permissible. A major source of concern and contention, for example, is the recent construction and planned expansion of hydroelectric dams,

* Corresponding author.
E-mail address: gang.chen@uncc.edu (G. Chen).

http://dx.doi.org/10.1016/j.apgeog.2015.06.001
0143-6228/

especially in the Amazon basin. On the one hand, the basin is shared by eight developing countries (Bolivia, Brazil, Colombia, Ecuador, Guyana, Peru, Suriname and Venezuela) with more than 340 million inhabitants. The remaining untapped hydroelectric potential in the area is expected to provide 'clean' energy to meet the regional rising demand for economic development (Tundisi, Goldemberg, Matsumura-Tundisi, & Saraiva, 2014). At present, 137 new hydroelectric dams have been planned in addition to the current list of 100 dams that are in operation (Tundisi et al., 2014). On the other hand, there are arguments that the operation of dams may lead to variations in the hydrological, land-use, climatic, and edaphic variables, resulting in forest decline and loss (Ferreira, Cunha, Chaves, Matos, & Parolin, 2013; Finer & Jenkins, 2012; Stave, Oba, Stenseth, & Nordal, 2005).

In the past decade, research efforts in tropical forest conservation have shifted towards studying the important temporal role of anthropogenic impacts on forest ecosystems as well as the development of a better understanding and evaluation of forest change in the context of dam operation. Specifically, several studies have focused on the carbon emissions caused by forest inundation in the hydroelectric reservoirs. For example, both Fearnside (2005) and Abril, Parize, Pérez, and Filizola (2013) found that flooded biomass can produce abundant carbon dioxide and methane that are a large and previously unrecognized source of greenhouse gas emissions. Several other researchers argued that the impact of hydroelectric dams extends well beyond the area surrounding the reservoirs, with forest stress and decline discovered in upstream and downstream ecosystems from dams (Ford and Brooks Rene, 2002; Horton & Clark, 2001; Manyari & de Carvalho, 2007; Palmeirim, Peres, & Rosas, 2014). This phenomenon could be partially explained by the lack of successful regeneration of native species as a result of hydrological change (Horton & Clark, 2001). Finer and Jenkins (2012) further examined the potential ecological impacts of planned hydroelectric dams across major Andean tributaries of the Amazon River. Their modeling results suggested that the lack of a strategic plan to build a series of new dams could lead to a severe break in river connectivity, driving deforestation in the Amazon basin.

Most of the previous studies relied primarily on sample-based field observations to assess the ecological impact of hydroelectric dams. While the findings added knowledge to improving our understanding of forest vulnerability, the spatially and temporally detailed patterns of forest change in the vicinity of the mega-structures remain to be analyzed, precluding an accurate landscape-level evaluation of the forest–dam relationship in the Amazon basin. Here, we provide a case study combining remote sensing, GIS and statistical analysis to extract and evaluate the spatially-explicit patterns of deforestation and forest degradation in the Brazil's Tucuruí Dam region over a period of 25 years from 1988 to 2013. The Tucuruí Dam was the first large-scale hydroelectric project in the Amazon region, an ideal case for understanding the long-term impact of mega-dams on rainforest loss. In this research, we aim to address two main questions at the landscape level: (i) What were the rates of deforestation and forest degradation that occurred within the large Tucuruí Dam region over time? (ii) Whether deforestation and forest degradation follow similar spatiotemporal patterns across three areas, including the neighborhoods of the dam, river upstream of the dam, and river downstream of the dam?

2. Materials and methods

2.1. Study area

The Tucuruí Dam (03°49′54″S, 49°38′48″W) is centered in our study area, a region of 80,000 km^2 in the State of Pará, Brazil (Fig. 1). This hydropower plant was the first of a series of 15 plants to be installed in the heart of the Amazon's Araguaia-Tocantins hydrographic basin (Manyari & de Carvalho, 2007). The phase I construction of the Tucuruí Dam was completed in 1984, creating a reservoir that flooded an area of 2850 km^2 (Porvari, 1995). With the recent completion of phase II, the dam has a maximum capacity of generating 8370 MW (megawatts) of electricity, to be supplied to the Northeast and Center-West regions of Brazil through high-tension transmission lines (Manyari & de Carvalho, 2007). The tropical forests in the region experienced a high degree of fragmentation. Some trees, on account of their proximity to the reservoir area, were lost, while deforestation and forest degradation were also observed around the dam (Fearnside, 2002; Manyari & de Carvalho, 2007).

2.2. Data acquisition and pre-processing

Remote sensing Landsat images were acquired from the U.S. Geological Survey archive in the dry season (July and August) of 1988, 1995, 2001, 2008 and 2013, spanning 25 years. Specifically, the 1988, 1995, and 2008 data were collected by the Landsat 5 TM sensor. The 2001 data were acquired by Landsat 7 ETM+, while the 2013 data were captured using the most-recent Landsat 8 OLI sensor launched in early 2013. Although multiple sensors served in data acquisition, the image extent, spatial resolution, geometry, spectral characteristics, and data quality remained consistent thanks to the consistency of the 40 + year Landsat program (Roy

Fig. 1. The Tucuruí Dam (03°49′54″S, 49°38′48″W) is centered in our study area, a region of 80,000 km^2 in the state of Pará, Brazil.

et al., 2014). In order to cover the entire study area of 80,000 km^2, four adjacent image scenes were collected at each of the five time steps (path/row: 223/62, 224/62, 224/63, and 223/63) with a total of 20 scenes downloaded. The high percentage of cloud cover in the tropics created challenges for acquiring clear-sky images from all the desired years. Three image scenes were replaced using the neighboring-year data with less than 5% of cloud cover. The rationale of our date selection was based upon the consideration of obtaining low cloud coverage imagery (less than 5%) in the entire region with comparable time intervals. Please note that there is currently no specific criterion regarding what temporal threshold should be used to monitor long-term forest loss (Herold et al., 2011).

Radiometric correction of the Landsat images included two major steps. First, digital numbers (DNs) were converted to at-sensor radiances, which were then converted to top-of-atmosphere (TOA) reflectance (Chen, Wulder, White, Hilker, & Coops, 2012). Second, atmospheric distortions were reduced by the popular 6S (Second Simulation of the Satellite Signal in the Solar Spectrum) radiative transfer model to derive surface reflectance (Vermote, Tanre, Deuze, Herman, & Morcrette, 1997). NASA's MODIS (Moderate Resolution Imaging Spectroradiometer) atmospheric products of aerosol optical thickness and water vapor were employed as model input. For the images acquired during the time periods when the atmospheric products were not available, they were normalized to an atmospheric corrected image using linear scale invariance of the multivariate alteration detection (MAD) transformation that can identify invariant pixels (Canty, Nielsen, & Schmidt, 2004). Geometric correction was not performed because the multitemporal images from the Landsat archive already had sub-pixel geolocation accuracies (Kennedy, Yang, & Cohen, 2010). Image masking was conducted to exclude water, thick clouds, cloud shadows, and impervious surfaces from the succeeding image analyses, with thresholds heuristically defined for every image scene. Finally, we mosaicked the four adjacent image scenes at each time step and clipped the mosaics to a square area of 80,000 km^2, where the Tucuruí Dam located at the center.

2.3. Extraction of deforestation and forest degradation

Deforestation is known as the process of tree cover loss below the threshold of a chosen forest definition for the purpose of timber production or land conversion. Forest degradation, however, does not have a globally accepted definition, but is usually referred to as a net loss of carbon stock or reduction of stem density in remaining forest land (Goetz et al., 2009; GOFC-GOLD, 2014). At the spatial resolution of 30 m, Landsat imagery is sufficient to detect large-scale deforestation, but is too coarse to directly reveal the degree of forest degradation that typically occurs at the sub-pixel level. In this research, we applied a spectral mixture analysis (SMA) approach AutoMCU (Automated Monte Carlo Unmixing) to extract the fractions of three major components (i.e., endmembers) – photosynthetic vegetation (PV), non-photosynthetic vegetation (NPV) and bare soil (Soil) – from individual image pixels in the CLASlite environment, with an aim to quantify sub-pixel canopy loss (Asner & Heidebrecht, 2002). Most of the SMA approaches, including AutoMCU, are based on the assumption that the value of each image pixel (i.e., reflectance) is the linear combination of the reflectance from PV, NPV, and bare soil weighted by their fractions in a forest environment (Eq. (1)).

$$P_{i,j} = P_{\mathrm{PV},i}F_{\mathrm{PV},j} + P_{\mathrm{NPV},i}F_{\mathrm{NPV},j} + P_{\mathrm{Soil},i}F_{\mathrm{Soil},j} + R_{i,j} \quad (1)$$

where $P_{i,j}$ is the reflectance in the i-th band of the j-th pixel, P contains the spectra of each endmember (PV, NPV, or Soil), F contains the fractional contribution (between 0 and 1) of each endmember spectrum to each pixel, and R is an error term. There are two attractive features in AutoMCU. First, the spectral reflectance libraries used by AutoMCU contain a diverse range of soil types, surface organic matter levels, and moisture conditions from more than 400,000 field and spaceborne (i.e., NASA's Hyperion) spectrometer observations collected in tropical forests throughout Central and South America as well as the Pacific Islands (Asner, Knapp, Balaji, & Páez-Acosta, 2009). Second, the spectra of PV, NPV and Soil are iteratively selected from the libraries in a random manner (i.e., a Monte Carlo approach) to determine the endmember spectra in each image scene (when reaching stable standard deviations), with root mean squared errors (RMSEs) also calculated to facilitate model performance evaluation (Asner et al., 2009).

Following the application of AutoMCU, we employed two decision trees to extract deforestation and forest degradation from each of the five time steps of Landsat images acquired in 1988, 1995, 2001, 2008 and 2013, with thresholds shown in Eq. (2) and Eq. (3).

$$F_{\mathrm{PV}t} < 56\% \quad (2)$$

$$56\% < F_{\mathrm{PV}t} < 80\% \text{ AND } 14\% < F_{\mathrm{NPV}t} < 34\% \text{ AND } 0\% < F_{\mathrm{Soil}t} < 17\% \quad (3)$$

where t represents each of the five time steps. It should be noted that several other decision trees were developed for monitoring tropical tree loss in previous studies. For example, Souza Jr. et al. (2003) constructed a classification tree to map degraded forests in Eastern Amazon using 20 m SPOT 4 (Satellite Pour L'observation de la Terre) imagery. The reason of adopting Eq. (2) and Eq. (3) in this research was because these decision trees have been thoroughly tested using extensively field-based validation in the tropics covering our study area (Asner et al., 2009, 2005). For instance, this approach has proven effective to quantify the amount of selective logging with an overall RMSE of 11–14% in the Amazon (Asner et al., 2005). To evaluate the mapping accuracy of deforestation and forest degradation in this study area, we randomly selected 50 validation plots (30 by 30 m) from a Google Earth Pro (Google Inc., California, USA) high-resolution Quickbird image (0.65 m pan-sharpened true color) collected in June 2013 covering a portion of the study area. We identified plot-level deforestation or forest degradation by following the protocol created by Gerwing (2002), who studied intact, logged and burned forests over the same region. Specific to the study area, canopy cover between 72% and 38% refers to degraded forests; while canopy cover lower than 38% indicates deforested land. Due to the lack of high-resolution imagery from previous years, we assumed that the accuracy of results remained relatively consistent throughout the time series and, thus, used the same set of decision tree criteria (Eq. (2) and Eq. (3)) for 1988, 1995, 2001, and 2008. This was also based on the fact that the surface reflectance of ground features remained relatively consistent over years.

2.4. Statistical analysis of the spatiotemporal patterns of canopy loss

The GIS proximity analysis was conducted to assess the influence of distance (to the dam region) on canopy loss. Specifically, we created multiple buffers around three locations of the Tucuruí Dam, river upstream of the dam, and river downstream of the dam in the ArcGIS environment (Esri, Redlands, California, USA), respectively. For the upstream forest ecosystem, we focused on the trees in the vicinity of the large reservoir formed by dam construction. The distance between the farthest end of the reservoir and the dam was

approximately 130 km. For the downstream, we assessed the forests as far as 190 km down the river nearby the City of Cametá, where the Tocantins River became wider and gradually merged into Baía de Marajó. We created multiple buffers from 5 km to 80 km at an equal interval of 5 km, resulting in a total of 16 buffer rings around each of the three evaluated locations.

We conducted three groups of statistical hypothesis testing (i.e., the Friedman test, the Wilcoxon signed-rank test, and the chi-square test) to investigate whether the loss of trees differed significantly across four time periods (i.e., 1988–1995, 1995–2001, 2001–2008 and 2008–2013), across three disturbance locations (i.e., dam neighborhoods, upstream reaches, and downstream reaches), and between two disturbance types (i.e., deforestation and forest degradation). For the purpose of meeting the statistical assumption of data independence, we randomly selected 10% of all pixels from a Landsat image mosaic, and used these sample locations to extract deforestation and forest degradation from the results in Section 2.3. This was followed by the calculation of the percentages of tree loss within individual buffer rings, i.e., the number of deforestation or forest degradation samples divided by the number of all samples in each ring. The rates of deforestation and forest degradation were extracted by dividing the percentages of tree loss the number of years for each time step.

Of the three significance tests, first, the Friedman test was employed to compare the median deforestation rates (as a function of distance discretized by the buffer rings) among the four time periods. The same analysis was also applied to assess the differences in forest degradation among the four time phases. Here, the nonparametric Friedman test was selected as an alternative to the typical one-way ANOVA (analysis of variance) with repeated measures, because the distributions of the rates of deforestation or forest degradation were found to frequently violate the assumption of normality based upon our preliminary assessments (Hollander & Wolfe, 1999). This was also the main reason why only nonparametric tests were employed in the succeeding significance tests. The null hypothesis for all the Friedman tests was that the median rates of deforestation or forest degradation among sample groups were equal. Second, we applied the Wilcoxon signed-rank test, the nonparametric version of a paired samples *t*-test (Hollander & Wolfe, 1999), to compare the mean rates of deforestation or forest degradation between each two pairs of the three disturbance locations. The null hypothesis was that the mean rates of deforestation or forest degradation around any two of the locations were equal. Finally, we used the chi-square test to compare the distributions (i.e., spatial patterns) of deforestation and forest degradation as a function of distance. We did not conduct a significant test on the mean rates of deforestation and forest degradation, because our preliminary results revealed a considerably higher level of deforestation as compared to degradation during all the four time periods. Here, the utilization of the chi-square test allowed us to explore whether the two types of disturbances followed the similar spatial patterns as the function of distance to the dam, river upstream, and river downstream, under the null hypothesis that the sample groups had the same distribution (Hollander & Wolfe, 1999).

3. Results and discussion

3.1. Mapping deforestation and forest degradation

The overall accuracy of the 2013 deforestation and forest degradation map was 78.0%, with the Kappa statistic of 0.77 (Table 1). Specifically, classification of intact forests with typically closed canopies achieved the highest accuracies (users: 85.0%; producers: 85.0%). Errors and uncertainties were mainly introduced when identifying disturbed forests. For example, tropical plants were not evenly regenerated in some large clear cuts, where the image spectral reflectance was the mixture of bare soil and healthy vegetation. Those previously deforested patches were possibly misclassified as degradation. In fact this is a scale issue, where scattered and regenerated vegetation caused spectral 'noises' in large logged lands. We also observed an edge effect, where trees on the boundaries of forest stands were misclassified as degraded forests. The relatively low resolution Landsat data precluded an accurate extraction of spatial patterns within the 30 m image grids. Another source of error may be caused by the nonlinear nature of spectral reflectance from the ground features. Although linear mixture models have been widely used in many studies, including ours, a nonlinear pixel unmixing process may better reflect the reality (Raksuntorn & Du, 2010).

The mapping results illustrated varying patterns of deforestation and forest degradation over the four time periods from 1988 to 2013. Specifically, deforestation led to the loss of 4341, 4135, and 4618 km^2 of forests in the first three time periods, i.e., 1988–1995, 1995–2001, and 2001–2008, at the rates of 620, 591, and 660 km^2 per year (Fig. 2). The amounts of canopy loss were relatively consistent, with a standard deviation of 35 km^2 per year (5.3% of the average). Surprisingly, the amount of deforestation dramatically decreased during the most recent time period 2008–2013, totaling 1624 km^2 at the rate of 325 km^2 per year (Fig. 2). This deforestation rate is less than half of what typically occurred during the two decades preceding 2008. The spatial patterns of deforestation as shown in Fig. 3 indicate that the continuity of forest loss over the period of 25 years were mainly caused by anthropogenic activities, such as human settlement and resettlement (e.g., road and building construction, and land conversion from forest to agriculture) and logging. This makes sense, because in 1970, the population of the town of Tucuruí was approximately 10,000; however, it dramatically rose to about 61,000 by 1980 mainly due to the recruitment and settlement of workers for dam construction (Manyari & de Carvalho, 2007). Additionally, lands were needed for the relocation and resettlement of the residents (around 25,000 and 35,000) who formerly lived in the areas inundated by the post-construction artificial reservoir (La Rovere & Mendes, 2000). By 2014, the total population of Tucuruí was estimated to be greater than 105,000, a 950% increase in 40 years (City Population, 2014). The inset of Fig. 3 clearly demonstrates the conversion of lands from forest to agriculture, where deforested patches are large with regular square shapes. The observed fishbone patterns in Fig. 3 further denote logging activities close to major roads and alongside the upstream reservoir. With new roads constructed to connect evergrowing cities around the dam, timber production also became economically feasible. Besides persistent forest loss, we found that the rate of deforestation remarkably declined from 656 km^2 per year to 325 km^2 per year starting from about 2008 (Fig. 2). Two main reasons may have contributed to this decline. First, the 2008 global economic crisis affected almost every aspect of the economic activities in Brazil, especially the ones related to exportation, such as logging and saw wood production (Canova & Hickey, 2012). Second, the Brazilian Law of Environmental Crimes was promulgated in 1998, with an aim to protect wildlife and plants of the country from environmental crimes, e.g., deforestation [Federal Law No. 9.605, Government of Brazil (1998)]. The subsequent regulation (Federal Decree No. 6.514) states that the enforcement of this law commences on July 22nd, 2008 (Government of Brazil, 2008). Reduced rate of tree loss in the Amazon was also evident in other studies. For example, Nepstad, Soares-filho, Merry, Lima, et al. (2009) found that deforestation in the Brazilian Amazon declined to 36% of its historical levels in the late 2000s (see Fig. 4).

Table 1
Accuracy of deforestation and forest degradation mapping in 2013.

User class	Reference class				
	Intact forest	Deforestation	Forest degradation	Total	User's accuracy (%)
Intact forest	17	0	3	20	85.0
Deforestation	1	13	1	15	86.7
Forest degradation	2	4	9	15	60.0
Total	20	17	13	50	
Producer's Accuracy (%)	85.0	76.5	69.2		
Overall accuracy (%) = 78.0					
Kappa statistic = 0.77					

Compared to deforestation, forest degradation was more constant during the entire 25-year period, with 701, 471, 628, and 695 km^2 of trees affected during the four time periods, respectively (Fig. 2). The average rate of forest degradation was 102 km^2 per year or 17.8% of the average rate of deforestation (~573 km^2 per year). Forest degradation reached its highest rate between 2008 and 2013, which is different from the temporal dynamics as previously discovered in deforestation mapping (Fig. 2). This phenomenon is linked to persistent selective logging in the region prompted by recent governmental incentives to Sustainable Forest Management. It may also be partially associated with the fact that human-driven land-cover changes have an overwhelmingly detrimental effect on forest diversity (e.g., species richness) making trees more vulnerable to the succeeding disturbances causing degradation (Gibson et al., 2011).

3.2. Comparing the spatiotemporal patterns of deforestation and forest degradation

The median rates of deforestation were found to be significantly different across the four time periods within the neighborhoods of all the three locations, i.e., the dam, the river downstream and the river upstream (p-values<0.005; Table 2). However, when the Friedman test was applied to the first three time periods from 1998 to 2008, we found no significant difference around the dam (p-value = 0.284), downstream reaches (p-value = 0.087), and upstream reaches (p-value = 0.472). This indicates that the rate of deforestation was significantly reduced during the final time period (2008–2013) for all three sub-regions. For example, the median rate of deforestation was 0.37% per year around the dam during the final time period, while such rate was averaged at 1.00% prior to 2008 (Fig. 5). Especially for the regions close to the dam or river upstream (e.g., within the buffer of 20 km), it was evident that the rates of deforestation were remarkably reduced to less than one third of the historical medians (Fig. 5). While the aforementioned global economic crisis and national policy (Section 3.1) likely played a pivotal role in reducing deforestation, we also noticed that intensely developed areas left fewer intact forests stands available for large-scale logging and human settlement. This may well explain the temporal deforestation pattern around the less-developed river downstream (Fig. 3), where the reduction of

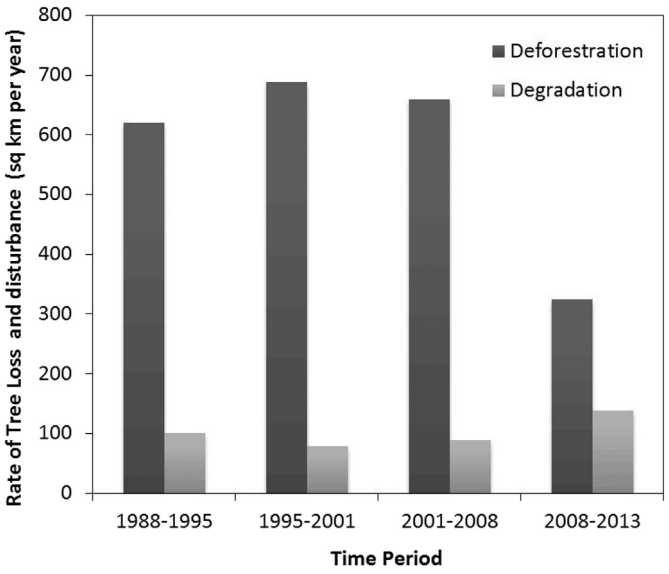

Fig. 2. The rates of deforestation and forest degradation over the four time periods from 1988 to 2013.

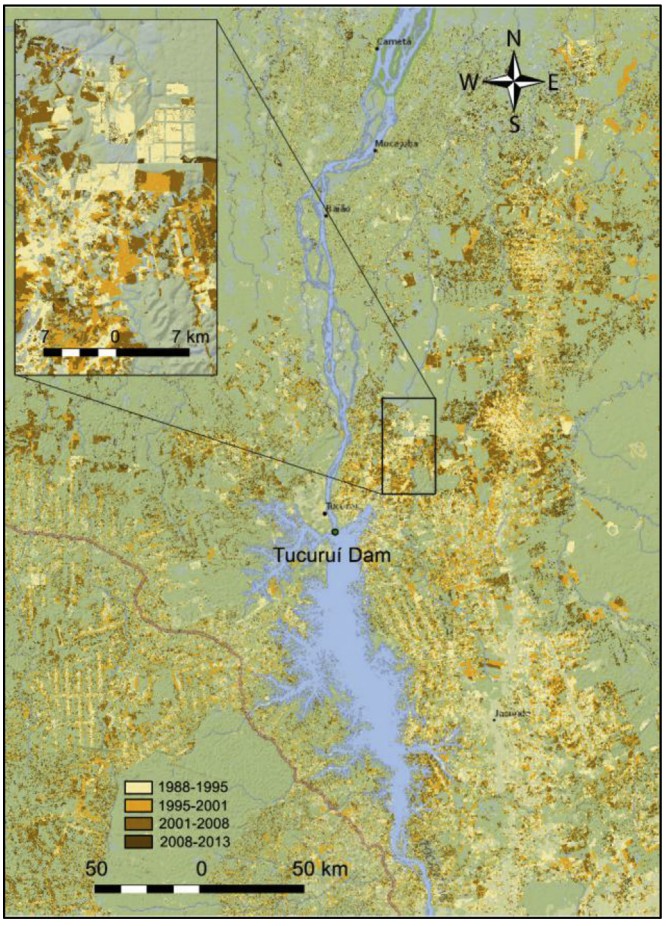

Fig. 3. Deforestation map showing the spatial patterns of major tree loss over the four time periods from 1988 to 2013.

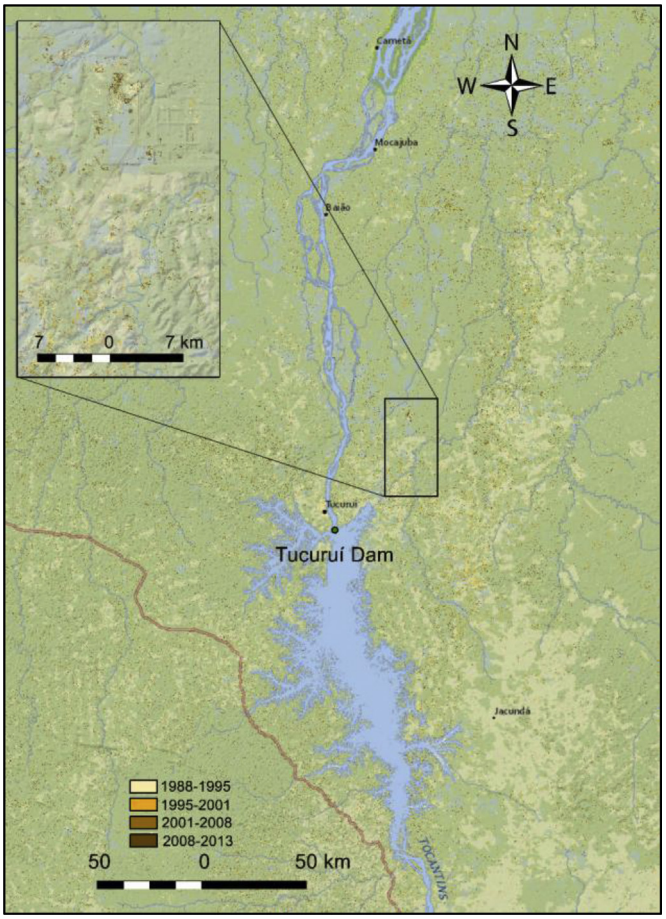

Fig. 4. Degradation map showing the spatial patterns of degraded trees over the four time periods from 1988 to 2013.

deforestation during the last time period was not as significant as these around the other two locations (Fig. 5).

Similar to the temporal patterns of deforestation, forest degradation was found to be significantly different across the four time periods within the neighborhoods of all the three locations (p-values<0.005; Table 2). However, degradation was more variable than deforestation, where significant differences were also found among the first time periods (p-values<0.005). It was unexpected that forest degradation between 2008 and 2013 showed the highest rates across the four time periods in the neighborhoods of all the three locations (Fig. 5).

The Wilcoxon signed-rank test was employed to assess whether deforestation or forest degradation varied significantly from the neighborhoods of one location to another during the same time periods. We found that, the rates of deforestation were significantly different (p-values<0.05; Table 3) between the dam and downstream neighborhoods, and between the downstream and upstream neighborhoods. However, an exception occurred during 2008–2013, when the mean rates of deforestation did not show significant difference around all the three locations (p-values>0.05; Table 3). We also compared the spatial patterns of deforestation across the buffer rings. In the upstream neighborhood, it was apparent that distance to the reservoir was a major factor reducing local canopy cover, i.e., the closer to the artificial reservoir the higher rate of tree loss was observed. Logging activities on both sides of the reservoir, as evident by the fishbone patterns, have been facilitated by the construction of several major roads (e.g., 422, 230, PA-151 and 150) that connect the expanding communities near the dam (Fig. 3). Similar results were found in the spatial patterns of forest degradation. For example, the average amount of degraded trees was less in the downstream region than those in the neighborhoods of the dam and the river upstream of the dam (Table 3).

We also evaluated whether deforestation and forest degradation followed similar spatial patterns (as a function of distance to each of the three locations). Surprisingly, all the chi-square tests gave the same result, i.e., no significant difference (p-values = 1.00). Such high agreement indicates that deforestation and forest degradation have interacted with each other both spatially and temporally around the dam, river upstream of the dam and river downstream of the dam. It was possible that human-induced major disturbances made forests more vulnerable to other anthropogenic and natural disturbances. For example, the major state roads can facilitate high accessibility to intact forests, possibly leading to more logging activities at the small patch level. Moreover, forest diversity is often reduced by human-driven land-cover changes, resulting in high forest vulnerabilities to other natural or human disturbances (Gibson et al., 2011). Degradation of soil and water conditions could have also caused tree mortality (Palmeirim et al., 2014) and contributed deforestation.

The neighborhoods used in this study ranged from 5 km to 80 km. It was found that the spatial patterns of tree loss (as a function of distance) for the three locations were different (Fig. 5). For example, the rate of deforestation decreased as the distance to the river upstream increased, while the rate of deforestation increased and then started to decrease at the distance of approximately 50 km within the neighborhoods of the dam. This phenomenon indicates that the impact of construction and operation of hydroelectric dams on forest cover change may follow varying spatial patterns. Forests that are immediately adjacent to the mega-dams may not necessarily suffer from the most severe disturbances, as unexpected spatial variation in hydrological, climatic, edaphic, as well as the land-use variables (e.g., road construction, and land conversion to agriculture) can affect ecological robustness (Ferreira et al., 2013; Finer & Jenkins, 2012; Stave et al., 2005). We further found that the distance-related patterns of tree loss remained relatively consistent across the four time periods (Fig. 5), suggesting that the long-lasting influence of existing and planned mega-dams could follow similar spatial trajectories in the absence of any major change in policies and/or disturbances.

Table 2
Comparison of the medians in canopy loss over the four time periods using the Friedman test.

Type of comparison	P-value
Four time periods around the dam	Deforestation: 0.000 Forest degradation: 0.003
Four time periods around the river downstream of the dam	Deforestation: 0.000 Forest degradation: 0.000
Four time periods around the river upstream of the dam	Deforestation: 0.001 Forest degradation: 0.000

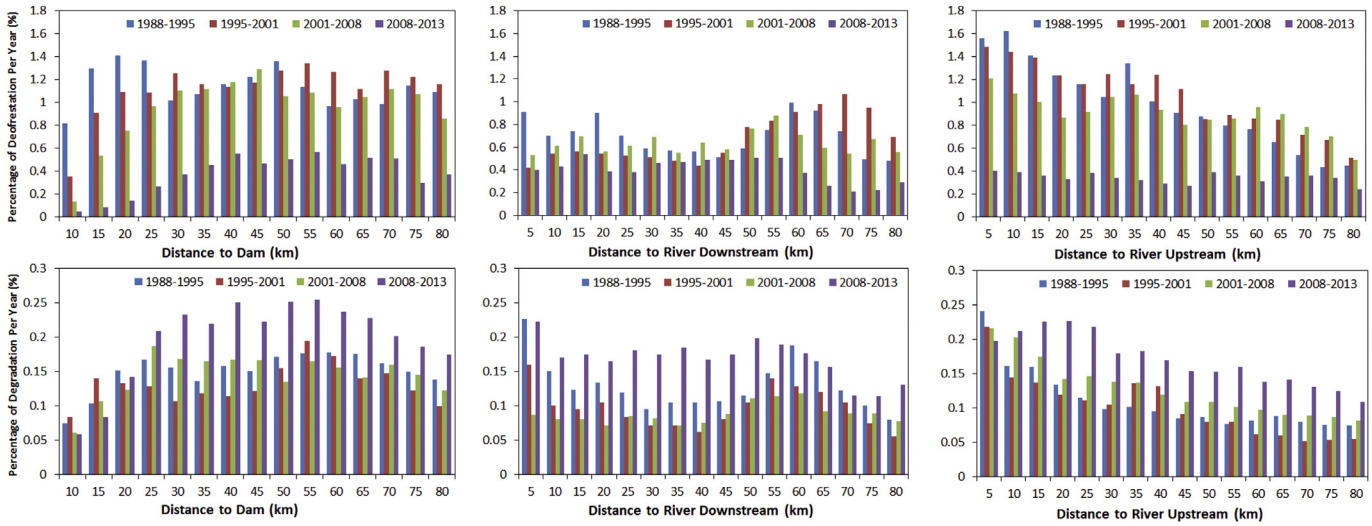

Fig. 5. Rates of deforestation and forest degradation around the dam, river downstream of the dam, and river upstream of the dam.

Table 3
Comparison of the means of canopy loss between each two pairs of the three disturbance locations, i.e., around the dam, around the river downstream of the dam, and around the river upstream of the dam, using the Wilcoxon signed-rank test.

Type of comparison	*P*-value
Dam *vs.* river downstream	Deforestation: 0.008[a]/0.002[b]/0.023[c]/0.501[d] Forest degradation: 0.109[a]/0.008[b]/0.003[c]/0.255[d]
Dam *vs.* river upstream of the dam	Deforestation: 0.163[a]/0.569[b]/0.352[c]/0.717[d] Forest degradation: 0.063[a]/0.079[b]/0.234[c]/0.501[d]
River downstream of the dam *vs.* river upstream of the dam	Deforestation: 0.011[a]/0.020[b]/0.001[c]/0.070[d] Forest degradation: 0.049[a]/0.679[b]/0.017[c]/1.000[d]

[a] 1988–1995.
[b] 1995–2001.
[c] 2001–2008.
[d] 2008–2013.

4. Conclusions

Understanding how existing hydroelectric dams impact surrounding forests over time can provide vital insight for assessing the ecological implications of constructing similar mega-structures within the Amazon basin. In this case study, we investigated the spatial patterns of deforestation and forest degradation over a period of 25 years in an 80,000 km^2 area centering the Tucuruí Dam, the first large-scale hydroelectric project in the Amazon region. We found that the rates of deforestation were consistent during the first three time periods 1988–1995 (620 km^2 per year), 1995–2001 (591 km^2 per year), and 2001–2008 (660 km^2 per year). Settlement and resettlement associated anthropogenic disturbances (e.g., agriculture conversion, logging, and road expansion) play a major role causing tree loss. However, it is important to note that the deforestation rate from 2008 to 2013 was half of the historical level (325 km^2 per year). It is highly likely that this drop in deforestation rate can be linked to the 2008 global economic crisis and enforcement of the Brazilian Law of Environmental Crimes. Forest degradation was relatively stable during four time periods. The average rate of degradation was 17.8% of the rate of deforestation, but they followed similar spatial patterns from the immediate neighborhoods of the dam, river upstream of the dam or river downstream of the dam, to a distance of 80 km from these sites, respectively. While human-driven deforestation may lead to high forest vulnerability (e.g., degradation) to other disturbances, degradation in soil and water conditions due to dam operation may have also resulted in deforestation.

Our results further unveiled similar rates of canopy loss in the neighborhoods of the Tucuruí Dam and the neighborhoods of the river upstream. This was mainly attributed to the fast expansion of the Tucuruí town, and the intensive logging activities alongside the major roads in the vicinity of the upstream reservoir. In contrast, a significantly lower level of forest disturbance was discovered in the river downstream. Finally, we found that forests that were closer to the dam or river did not necessarily suffer from more severe disturbances, suggesting that hydrological, climatic, edaphic, and land-use variables possibly affect ecological robustness in various spatial patterns.

Acknowledgments

This research was supported by the North Carolina Space Grant New Investigators Award (NNX10A168H), the University of North Carolina at Charlotte's Junior Faculty Development Award, and the Natural Sciences and Engineering Research Council of Canada (NSERC) (471353-2015). The authors thank the anonymous reviewers for their valuable suggestions.

References

Abril, G., Parize, M., Pérez, M. A. P., & Filizola, N. (2013). Wood decomposition in Amazonian hydropower reservoirs: an additional source of greenhouse gases. *Journal of South American Earth Sciences, 44*, 104–107.
Asner, G. P., & Heidebrecht, K. B. (2002). Spectral unmixing of vegetation, soil and dry carbon cover in arid regions: comparing multispectral and hyperspectral observations. *International Journal of Remote Sensing, 23*, 3939–3958.

Asner, G. P., Knapp, D. E., Balaji, A., & Páez-Acosta, G. (2009). Automated mapping of tropical deforestation and forest degradation: CLASlite. *Journal of Applied Remote Sensing, 3*(1), 033543.

Asner, G. P., Knapp, D. E., Broadbent, E. N., Oliveira, P. J. C., Keller, M., & Silva, J. N. (2005). Selective logging in the Brazilian Amazon. *Science, 310*, 480–482.

Canova, N. P., & Hickey, G. M. (2012). Understanding the impacts of the 2007–08 global financial crisis on sustainable forest management in the Brazilian Amazon: a case study. *Ecological Economics, 83*, 19–31.

Canty, M. J., Nielsen, A. A., & Schmidt, M. (2004). Automatic radiometric normalization of multitemporal satellite imagery. *Remote Sensing of Environment, 91*, 441–451.

Chen, G., Wulder, M. A., White, J. C., Hilker, T., & Coops, N. C. (2012). Lidar calibration and validation for geometric-optical modeling with landsat imagery. *Remote Sensing of Environment, 124*, 384–393.

City Population. (2014). *The population development of Tucuruí*. Available online http://www.citypopulation.de/php/brazil-para.php?adm2id=M1508100.

Fearnside, P. M. (2002). Greenhouse gas emissions from a hydroelectric reservoir (Brazil's Tucuruí dam) and the energy policy implications. *Water Air Soil Pollut., 133*, 69–96.

Fearnside, P. M. (2005). Do hydroelectric dams mitigate global warming? the case of Brazil's Curuá Una dam. *Mitigation and Adaptation Strategies for Global Change, 10*, 675–691.

Ferreira, L. V., Cunha, D. A., Chaves, P. P., Matos, D. C. L., & Parolin, P. (2013). Impacts of hydroelectric dams on alluvial riparian plant communities in eastern Brazilian Amazonian. *Annals of the Brazilian Academy of Sciences, 85*, 1013–1023.

Finer, M., & Jenkins, C. N. (2012). Proliferation of hydroelectric dams in the Andean Amazon and implications for Andes-Amazon connectivity. *PLoS One, 7*, e35126.

Ford, C. R., & Brooks Rene, J. (2002). Detecting forest stress and decline in response to increasing river flow in southwest Florida, USA. *Forest Ecology and Managementrest, 160*, 45–64.

Fuller, J. L., Foster, D. R., McLachlan, J. S., & Drake, N. (1998). Impact of human activity on regional forest composition and dynamics in central New England. *Ecosystems, 1*, 76–95.

Gerwing, J. J. (2002). Degradation of forests through logging and fire in the eastern Brazilian Amazon. *Forest Ecology and Management, 157*, 131–141.

Gibson, L., Lee, T. M., Koh, L. P., Brook, B. W., Gardner, T. A., Barlow, J., et al. (2011). Primary forests are irreplaceable for sustaining tropical biodiversity. *Nature, 478*, 378–381.

Goetz, S. J., Baccini, A., Laporte, N. T., Johns, T., Walker, W., Kellndorfer, J., et al. (2009). Mapping and monitoring carbon stocks with satellite observations: a comparison of methods. *Carbon Balance and Management, 4*, 2.

GOFC-GOLD. (2014). *A sourcebook of methods and procedures for monitoring and reporting anthropogenic greenhouse gas emissions and removals associated with deforestation, gains and losses of carbon stocks in forests remaining forests, and forestation*. GOFC-GOLD Report version COP20-1. The Netherlands: GOFC-GOLD Land Cover Project Office, Wageningen University.

Government of Brazil. (1998). *Brazilian law of environmental crimes (Law No. 9.605 of February 12, 1998)*. Available online (in Portuguese) http://www.planalto.gov.br/ccivil_03/leis/l9605.htm.

Government of Brazil. (2008). *Administrative environmental misdemeanours law (Decree No. 6.514 of July 22, 2008)*. Available online (in Portuguese) http://www.planalto.gov.br/ccivil_03/_ato2007-2010/2008/decreto/D6514.htm.

Hansen, M. C., Potapov, P. V., Moore, R., Hancher, M., Turubanova, S. A., Tyukavina, A., et al. (2013). High-resolution global maps of 21st-century forest cover change. *Science, 342*, 850–853.

Herold, M., Román-Cuesta, R. M., Heymell, V., Hirata, Y., Van Laake, P., Asner, G. P., et al. (2011). A review of methods to measure and monitor historical carbon emissions from forest degradation. *Unasylva, 238*(62), 16–24.

Hollander, M., & Wolfe, D. A. (1999). *Nonparametric statistical methods*. Hoboken, NJ: John Wiley & Sons, Inc.

Horton, J. L., & Clark, J. L. (2001). Water table decline alters growth and survival of *Salix gooddingii* and *Tamarix chinensis* seedlings. *Forest Ecology and Management, 140*(2–3), 239–247.

Kennedy, R. E., Yang, Z., & Cohen, W. B. (2010). Detecting trends in forest disturbance and recovery using yearly landsat time series: 1. LandTrendr – temporal segmentation algorithms. *Remote Sensing of Environment, 114*, 2897–2910.

La Rovere, E. L., & Mendes, F. E. (2000). *Tucuruí hydropower complex, Brazil, A WCD case study prepared as an input to the World Commission on Dams, Cape Town*. Available online http://www.internationalrivers.org/files/attached-files/csbrmain.pdf.

Lambin, E. F. (1997). Modelling and monitoring land-cover change processes in tropical regions. *Progress in Physical Geography, 21*, 375–393.

Manyari, W. V., & de Carvalho, O. A. (2007). Environmental considerations in energy planning for the Amazon region: downstream effects of dams. *Energy Policy, 35*(12), 6526–6534.

Nepstad, D., Soares-filho, B. S., Merry, F., Lima, A., Moutinho, P., Carter, J., et al. (2009). The end of deforestation in the Brazilian Amazon. *Science, 36*, 1350–1351.

Palmeirim, A. F., Peres, C. A., & Rosas, F. C. W. (2014). Giant otter population responses to habitat expansion and degradation induced by a mega hydroelectric dam. *Biological Conservation, 174*, 30–38.

Pan, Y., Birdsey, R. A., Fang, J., Houghton, R., Kauppi, P. E., Kurz, W. A., et al. (2011). A large and persistent carbon sink in the world's forests. *Science, 333*, 988–993.

Porvari, P. (1995). Mercury levels of fish in Tucuruí hydroelectric reservoir and in river Mojú in Amazonia, in the state of Pará, Brazil. *Science of the Total Environment, 175*, 109–117.

Raksuntorn, N., & Du, Q. (2010). Nonlinear spectral mixture analysis for hyperspectral imagery in an unknown environment. *IEEE Geoscience and Remote Sensing Letters, 7*, 836–840.

Roy, D. P., Wulder, M. A., Loveland, T. R., Woodcock, C. E., Allen, R. G., Anderson, M. C., et al. (2014). Landsat-8: science and product vision for terrestrial global change research. *Remote Sensing of Environment, 145*, 154–172.

Saatchi, S. S., Harris, N. L., Brown, S., Lefsky, M., Mitchard, E. T. A., Salas, W., et al. (2011). Benchmark map of forest carbon stocks in tropical regions across three continents. *Proceedings of the National Academy of Sciences of the United States of America, 108*, 9899–9904.

Souza, C., Jr., Firestone, L., Silvaa, L. M., & Roberts, D. (2003). Mapping forest degradation in the eastern Amazon from SPOT 4 through spectral mixture models. *Remote Sensing of Environment, 87*, 494–506.

Stave, J., Oba, G., Stenseth, N. C., & Nordal, I. (2005). Environmental gradients in the Turkwel riverine forest, Kenya: hypotheses on dam-induced vegetation change. *Forest Ecology and Management, 212*, 184–198.

Tundisi, J. G., Goldemberg, J., Matsumura-Tundisi, T., & Saraiva, A. C. F. (2014). How many more dams in the Amazon? *Energy Policy, 74*, 703–708.

Uriarte, M., Canham, C. D., Thompson, J., Zimmerman, J. K., Murphy, L., Sabat, A. M., et al. (2009). Natural and human disturbance land use as determinants of tropical forest results from a forest simulator dynamics: results from a forest simulation. *Ecological Monographs, 79*, 423–443.

Vermote, E. F., Tanre, D., Deuze, J. L., Herman, M., & Morcrette, J.-J. (1997). Second simulation of the satellite signal in the solar spectrum, 6S: an overview. *IEEE Transactions on Geoscience and Remote Sensing, 35*, 675–686.